

Chandra Observations of the Anomalous X-ray Pulsar 4U 0142+61

Sandeep K. Patel¹, Chryssa Kouveliotou^{2,3}, Peter M. Woods², Allyn F. Tennant³,
Martin C. Weisskopf³, Mark H. Finger², Colleen Wilson-Hodge³, Ersin Göğüş⁴,
Michiel van der Klis⁵, Tomaso Belloni⁶

ABSTRACT

We present X-ray imaging, timing, and phase resolved spectroscopy of the anomalous X-ray pulsar 4U 0142+61 using the *Chandra X-ray Observatory* (CXO). The spectrum is well described by a power law plus blackbody model with $\Gamma = 3.35(2)$, $kT_{\text{BB}} = 0.458(3)$ keV, and $N_{\text{H}} = 0.91(2) \times 10^{22}$ cm⁻²; we find no significant evidence for spectral features (0.5 – 7.0 keV). Time resolved X-ray spectroscopy shows evidence for evolution in phase in either Γ , or kT_{BB} or some combination thereof as a function of pulse phase. We derive a precise X-ray position for the source and determine its spin period, $P = 8.68866(30)$ s. We have detected emission beyond 4'' from the central source and extending beyond 100'', likely due to dust scattering in the interstellar medium.

Subject headings: pulsars:individual (4U 0142+61) — stars:neutron — X-rays:stars

1. Introduction

4U 0142+61 was discovered in 1978 with *Uhuru* (Forman et al. 1978), but only in 1984 were 8.7-s pulsations detected in its persistent X-ray flux with *EXOSAT* (Israel, Mereghetti, & Stella 1994). Pulse frequencies were sparsely measured until the last few years. The

¹National Academy of Sciences-NRC/NSSTC, SD-50, Huntsville, AL 35805

²Universities Space Research Association/NSSTC, SD-50, Huntsville, AL 35805

³NASA Marshall Space Flight Center, Huntsville, SD-50, AL 35812

⁴Department of Physics, University of Alabama in Huntsville/NSSTC-SD50, Huntsville, AL 35805

⁵Astronomical Institute "Anton Pannekoek," University of Amsterdam, and Center for High Energy Astrophysics, Kruislaan 403, 1098 SJ Amsterdam, Netherlands

⁶Osservatorio Astronomico di Brera, Via Bianchi 46, 23807 Merate (Lc), Italy

frequency values are consistent with a constant spin-down rate of $\dot{\nu} = (-3.0 \pm 0.1) \times 10^{-14}$ Hz s⁻¹, slightly larger than the $\dot{\nu} = (-2.598 \pm 0.002) \times 10^{-14}$ Hz s⁻¹ recently measured with *RXTE* phase connected data (Gavriil & Kaspi 2001). Despite detailed searches (Israel, Mereghetti, & Stella 1994; Wilson et al. 1999), no evidence for orbital Doppler shifts has been found in the pulse frequency measurements. Upper limits of $a_X \sin i \lesssim 0.26$ lt-s for orbital periods in the range 70 s to 2.5 days (Wilson et al. 1999) place stringent limits on allowed orbital inclinations and companion masses for normal or helium main sequence companions.

ASCA observations in 1994 (White et al. 1996) and in 1998 (Paul, Kawasaki, Dotani, & Nagase 2000), both determined the source energy spectrum as an absorbed power law (photon index ~ 3.7) with a blackbody ($kT \sim 0.4$ keV) component. The *ASCA* GIS data also revealed very stable (in time) pulse profiles and intensities. The pulse profiles, however, evolved with energy from double-peaked (0.5-4.0 keV), to single peaked (4.0-8.0 keV) (White et al. 1996). Later spectral observations with *BeppoSAX* in 1997-1998 (Israel et al. 1999) were consistent with the *ASCA* spectral results, however it did not show significant pulse phase dependence. Using *RXTE* observations, Gavriil & Kaspi (2001) reported pulse profile evolution with energy, evolving from double-peaked (2.0–4.0 keV) to single peaked (6.0–8.0 keV). Juett et al. (2002) used the High Energy Transmission Grating Spectrometer (HETG) on the CXO to observe the source in 2001. They find no evidence for emission or absorption lines in the spectrum which is well fitted by an absorbed powerlaw+blackbody with $\Gamma = 3.3(4)$ and $kT = 0.418(13)$ keV. Their analysis used only phase averaged spectra and provided stringent constraints on spectral features.

Recent optical observations (Hulleman, van Kerkwijk, & Kulkarni 2000) have revealed an object with peculiar optical colors inside the *Einstein* error circle (White et al. 1987). The optical observations imply an extinction of $2.7 \lesssim A_V \lesssim 5.0$ and a distance of $d \gtrsim 2.7$ kpc. The object is too faint to be a large accretion disk. Further observations of the optical counterpart revealed pulsations with a 30% pulse fraction (Kern & Martin 2001). The large pulse fraction also rules out X-ray reprocessing (in a disk) as the source of the optical pulsations. A deep radio search showed no evidence for a SNR, extended structure, or even a point source at the position of 4U 0142+61 (Gaensler et al. 2001).

We present here an analysis and discussion of our *Chandra* observation of the source. In §2 we describe the x-ray observations, and present spatial, timing and spectral results of 4U 0142+61. We also include spatially resolved spectroscopy of the extended emission around 4U 0142+61, presumably due to dust scattering. A precise x-ray position is derived and compared with the optical identification from Hulleman, van Kerkwijk, & Kulkarni (2000).

2. Observations and Results

We observed 4U 0142+61 on 21 May 2000 with the *Chandra* Advanced CCD Imaging Spectrometer (ACIS). Data were collected sequentially in two different observing modes: timed exposure (TE) mode and continuous clocking (CC) mode. Data obtained in TE mode allow for two-dimensional imaging but not for accurate time averaged or pulse-phased spectroscopy due to pulse pile up and the low (3.24 s) time resolution of this data type. In CC mode the amount of pile up is negligible and one can exploit the 2.85 ms time resolution though the image is one-dimensional. The source was positioned on the nominal target position of ACIS-S3, a back illuminated CCD on the spectroscopic array (ACIS-S) with good charge transfer efficiency and spectral resolution.

Standard processing of the data was performed by the *Chandra* X-ray Center to Level 1 (CXC processing software version R4CU5UPD13.3). The *Chandra* calibration database (CALDB2.9) was utilized and the data were further processed using the CIAO (v2.2.1) tool *acis_process_events*. The data were filtered to exclude events with *ASCA* grades 1, 5, and 7, hot pixels, bad columns, and events on CCD node boundaries. The S3 light curve was inspected in a region offset from the AXP to identify times of high background rate. We binned the data in 200 s intervals and found no times when the background exceeded a 3σ threshold about the mean, and so all the data were deemed useful. The resulting observing times are 7744 s and 5945 s for TE and CC mode data, respectively. Uncertainties are reported at the 68% confidence level.

2.1. Timing Results

High resolution timing with ACIS is only possible using CC-mode data. The CC mode event times denote when the event was read out of the frame store, not when it was detected. We corrected for this effect by assuming that all photons were originally detected at the nominal target position. We removed the variable time delay due to spacecraft dither and telescope flexure. The event arrival times were then corrected to the solar system barycenter using the JPL planetary ephemeris DE-200.

The data were divided into ten intervals, each of ~ 600 s, and individual pulse profiles were created using a coarse ephemeris derived from an epoch fold search. These ten profiles were compared to the pulse profile derived using all the data and the relative phases were fit with a linear function. The resulting pulse period of 8.68866 ± 0.00030 s is referred to epoch MJD 551685.78. This period is consistent with the more precise spin history of the source determined with long term RXTE monitoring (Gavriil & Kaspi 2001).

Hereafter we use the entire dataset for our timing analysis. The pulse profile (0.5–7.0 keV) is shown in Figure 1a; the peak-to-peak pulse fraction ($PTP \equiv \frac{F_{\max} - F_{\min}}{F_{\max} + F_{\min}}$) is $6.7 \pm 0.9\%$. Here, F_{\max} and F_{\min} are the maximum and minimum count rates. We present in Figure 2 the variation in both the *rms* and peak-to-peak pulse fraction of the profile with energy. We find no significant variation of these values in three energy channels (0.1 – 1.3, 1.3 – 3.0, and 3.0 – 8.0 keV). However, we see evidence for evolution in the profile shape with energy (see §2.4 for quantitative details) with the first pulse being the softest.

2.2. AXP Position

We use only data collected in TE mode to derive the AXP position. For 4U 0142+61, which is rather bright (~ 21 ACIS counts/s between 0.5 – 7.0 keV), the data suffer from pile-up of photons in the image core, as a result of which the source image looks ring-shaped with a hole in the center. We modeled the data using a Gaussian multiplied by a hyperbolic tangent in radius, scaled to approach zero at $r = 0.0$ (Hulleman et al. 2001). The resulting best-fit centroids correspond, using the *Chandra* aspect solution, to a J2000 position on the sky of $\alpha = 01^{\text{h}}46^{\text{m}}22^{\text{s}}.42$, $\delta = +61^{\circ}45'02''.8$. The uncertainty is limited by systematic effects, to a circle with $\sim 0.7''$ radius (Aldcroft et al. 2000). This position is consistent with the location of the optical counterpart found by Hulleman, van Kerkwijk, & Kulkarni (2000), $\alpha = 01^{\text{h}}46^{\text{m}}22^{\text{s}}.41$, $\delta = +61^{\circ}45'03''.2$. Unfortunately, only one other (faint) X-ray source is visible in the TE observation. We were, therefore, unable to reduce the 4U 0142+61 positional error by using astrometry to obtain a boresight correction.

2.3. Extended Emission Search

While searching for extended emission (within a few arcseconds) one must account for numerous contributions to the observed flux. These contributions include not only the bright source itself and the instrumental background, but diffuse emission from the galactic plane, a dust scattering halo, and the potential contribution of an X-ray nebula.

To avoid issues related to the effects of pile up in the TE mode data, we first utilized the one dimensional image from the CC mode. We generated a time-integrated image (0.5 – 7.0 keV) minus any point sources other than 4U 0142+61. We then subtracted an average count rate intended to remove instrumental and diffuse cosmic X-ray background (Markevitch & Vikhlinin 2001, and references therein).

Next, we constructed what will be referred to as the “pulsed” image. We took the

observed pulse profile, normalized it to a mean of zero and convolved it with the event list of S3. Each count recorded on S3 was assigned a phase. Events with a phase near pulse maximum, regardless of their position on the chip, received a positive weight and likewise, those near pulse minimum, a negative weight. In doing so, we remove all emission components in our image that do not vary in phase (i.e., everything except the central pulsar). Note that the time delay for photons scattered by the interstellar dust is on average minutes, much longer than the pulsar period, and therefore will not contaminate the pulsed image.

To improve statistics, we then folded the 1-D time-integrated (CC_t) and pulsed (CC_p) images about the common centroid and accumulated “quasi-radial” profiles. These profiles are shown in Figure 3. We compare the pulsed radial profile with the MARX (Wise et al. 1997, v3.01) derived point spread function (PSF) and calculate $\chi^2/\nu = 15.2/8$. We conclude that the pulsed radial profile is consistent with the MARX PSF.

Next, we collapsed the TE mode observation to mimic the 1-D CC image (Figure 3, TE). We find that the TE profile completely overlaps the CC_t profile beyond $\sim 4''$, marking the radius beyond which the effects of pile-up are negligible. We conclude that the majority of the 4U 0142+61 X-ray flux is contained within a radius of $\sim 4''$.

In both profiles we find excess emission beyond $\sim 4''$ which is likely due to a dust-scattering halo and potentially an X-ray plerion. Azimuthally averaged radial profiles generated in different energy bands and spectra extracted from S3 in 3 concentric annuli centered on the pulsar position supports the dust scattering halo hypothesis. Detailed modelling of the spatial and spectral distribution of the dust scattered emission from a sample of X-ray bright sources, including 4U 0142+61, is underway and will be presented elsewhere.

2.4. Spectral Analysis

We use CC mode data to obtain an X-ray spectrum as these are not impacted by pile up. As no response calibration is currently available for *Chandra* CC mode data, here we assume that the CC and TE spectral responses are identical. To test this assumption, we compared spectra extracted from both CC and TE mode data. The extraction regions were selected from identical parts of the sky, more than $5''$ from 4U 0142+61, and close enough to the AXP to contain flux from the dust scattering halo. Background spectra were extracted from a region on S3 offset from this source region. All spectra and response files for our analysis were generated using the CIAO (v2.2.1) tools *dmextract*, *mkrmf*, and *mkarf*, and CALDB(v2.9). The extraction was performed in pulse invariant (PI) space

(*i.e.*, after the instrument gains were applied). We fit both CC and TE mode spectra with a TE mode response and an absorbed power law model; we found acceptable fits and reasonable agreement in the derived model parameters (CC: $N_{\text{H}} = 1.1 \pm 0.1$, $\Gamma = 3.2 \pm 0.2$, $\chi^2/\nu = 82.3/80$, and TE: $N_{\text{H}} = 1.1 \pm 0.1$, $\Gamma = 3.1 \pm 0.2$, $\chi^2/\nu = 84.8/103$). As a separate check, we subtract the CC mode spectra from the TE mode data and fit the difference to a constant. This fit resulted in a $\chi^2/\nu = 109.4/106$ and was consistent with zero. Based on these tests, we find it valid to adopt the TE mode response in our spectral analysis of the CC mode data.

We define the AXP source region by selecting an interval ± 8 pixels ($\pm \sim 4''$) (see also §2.3) around the peak flux along the collapsed CC mode axis. The background was determined using two adjacent segments 16 pixels wide for a total area 2 times the source area; the background flux contributes $\sim 1.7\%$ of the total (0.5-7.0 keV) flux in the source region.

The phase averaged spectrum of the source is shown in Figure 4. We have fit several models to the spectrum and we find that the best fit model is an absorbed power law + blackbody function, which gives $\Gamma = 3.40 \pm 0.06$, $kT_{\text{BB}} = 0.470 \pm 0.008$, with a hydrogen column density, $N_{\text{H}} = 0.93 \pm 0.02$. These parameter values are consistent with the values derived from simultaneous fits to phase resolved spectra (this is discussed in more detail later in this section). All spectral fits were limited to the 0.5 – 7.0 keV band with XSPECv11.01 (Arnaud 1996), and use the photo-electric absorption coefficients of Morrison & McCammon (1983), and abundances of Anders & Ebihara (1982).

Our results for N_{H} and Γ are consistent with the phase averaged results of Juett et al. (2002) derived from *Chandra* HETG data. However, the blackbody temperature derived here differs slightly (3.7σ) and is higher than the one derived from the HETG data. We do not view this difference as compelling since there are systematic effects that have been treated differently in the two analyses. The blackbody temperature derived here is also higher than the one derived using *ASCA* data (Paul, Kawasaki, Dotani, & Nagase 2000); the difference is likely due to contamination from the scattering halo within the large ($3'$ HPD) point spread function of the *ASCA* telescopes.

We search for evolution of the spectrum with pulse phase by systematically looking for significant variations in fitted spectral parameters as a function of pulse phase. Using the derived pulse period (§2.1) we construct a source spectrum for each of ten pulse phase bins. Each of the 10 resulting spectra were grouped into bins that contained at least 25 events.

We constrain the N_{H} to be identical at each phase (hereafter defined as “linked”), since we do not expect large variations in the absorption over the small angular size of the source

or any significant intrinsic absorption.

To confirm this assumption we perform and compare similar joint fits with (a) N_{H} free to acquire a best fit value in all phase bins and (b) N_{H} linked at each phase. All other model parameters are free to obtain their best fit values in each phase bin. We then fit the data from each of the ten pulse phase bins with an absorbed PL+BB model. The former method provides similar values of N_{H} for all bins and consistent with the linked value of $N_{\text{H}} = 0.91 \pm 0.02$ derived with the latter method. Furthermore, the former fit results in a $\Delta\chi^2 = 6.1$ for 9 additional parameters; an F -statistic probability of 78% is calculated, indicating that allowing N_{H} to be free does not statistically improve the fit.

Keeping N_{H} linked thereafter, we initially we fit the data with the power law normalization (PL_{Norm}), index (Γ), blackbody normalization (BB_{Norm}), and kT_{BB} free (Table 1, model 5); we found a $\chi^2/\nu = 1950.94/1779$. The fit is significantly improved ($\chi^2/\nu = 1491.469/1429$) by ignoring the 1.64 – 2.14 keV band, which contains the iridium-edge structure in the telescope response (2.04 keV) and the Si K fluorescence line (1.74 keV) and Si absorption edge (1.84 keV). (Current gain calibration is known to cause spurious features in high S/N spectra in this energy range⁷). One approach to dealing with this situation is to eliminate data from the analysis. However, to avoid eliminating data, we have opted for an alternative method of analysis. We included all events with energy between 0.5-7.0 keV and accounted for systematic errors by using the calculated reduced χ^2 (χ^2_{ν} to determine our 1- σ error bound. If $\chi^2_{\nu} \leq 1$ then the range of parameter space that encompasses a $\Delta\chi^2 = \pm 1$ is adopted as the 1- σ uncertainty; if $\chi^2_{\nu} > 1$ then the range of parameter space that encompasses a $\Delta\chi^2 = \pm\chi^2_{\nu}$ is adopted as the 1- σ uncertainty.

The above is the least restrictive constraint to the data and shows evidence for evolution with phase in kT_{BB} , but not in Γ . To investigate the evolution of spectral parameters, we perform a series of more constraining fits to the data.

We begin with an extremely restrictive fit where kT_{BB} and Γ are linked and the ratio of their normalizations is constant. The results of this fit are shown in Table 1 as model 1.

We next assume (Table 1, model 2) that the spectral shape is unchanged, but the contribution of each component varies. Consequently, we fit all phase bins with Γ and kT_{BB} linked, and allow the normalizations to vary. This fit results in a lower χ^2 as compared to model 1, ($\Delta\chi^2 = 16$, $\Delta\nu = 10$) which only improves the fit at the 84% confidence level. Hence, for the remaining fits we constrain the ratio of the normalizations to be linked.

Next, we keep Γ linked and allow kT_{BB} and the normalizations to vary (Table 1, model

⁷<http://asc.harvard.edu/udocs/>

3). The decrease in χ^2 here is significant ($\Delta\chi^2 = 34.2$, $\Delta\nu = 9$) indicating that allowing kT_{BB} to vary statistically improves the fit. The evolution of blackbody temperature is shown as a function of pulse phase in Figure 1b. The spread in kT_{BB} values is 0.032 keV.

The fits were repeated with kT_{BB} linked and with varying Γ and the normalizations (Table 1, model 4). The fit results in a $\Delta\chi^2 = 35.1$ ($\Delta\nu = 9$) which indicate that allowing Γ to vary, also statistically improves the fit. The evolution of the power law index is shown as a function of pulse phase in Figure 1c. The range of Γ variations here is 0.24. Models 3 and 4 indicate that there is evidence for evolution in phase in either Γ , or kT_{BB} or some combination thereof, as indicated by Table 1, model 5. The average 2–10 keV unabsorbed flux and X-ray luminosity, calculated using model 5, are 8.3×10^{-11} ergs $\text{s}^{-1} \text{cm}^{-2}$ and $0.99 d_{kpc}^2 \times 10^{34}$ ergs s^{-1} , respectively. The PL component contributes 61% to the 2–10 keV unabsorbed flux.

Finally, we have searched for spectral lines, but find no significant candidates. Features that appear below ~ 1 keV and in the Ir edge, are potentially due to uncertainty in the spectral response. To set upper limits, we examined two small deviations at 1.0 and 4.9 keV. The addition of a line, modeled by a Gaussian with an intrinsic width of 40 eV at 4.9 keV to the PL+BB model (Table 1, model 5), results in a $\Delta\chi^2 = 6.4$ for 3 additional parameters; an F –statistic probability of 95% is calculated, the 90% confidence upper limit on the line flux is 4.3×10^{-13} ergs $\text{cm}^{-2} \text{s}^{-1}$. Similarly, including a “line” at 1.0 keV results in a $\Delta\chi^2 = 4.4$ and an F –statistic probability of 86%. Our results are consistent with the results of Juett et al. (2002) derived from *Chandra* HETG data.

3. Discussion

We have observed the anomalous X-ray pulsar, 4U 0142+61 with *Chandra* and performed detailed phase resolved spectroscopy of the source. We find that there is significant spectral evolution during the overall pulse. The phase averaged spectrum can be best fit with a two component model (PL+BB), consistent with earlier results (Juett et al. (2002); White et al. (1996); Israel et al. (1999); Paul, Kawasaki, Dotani, & Nagase (2000)). We confirm the source location of Juett et al. (2002), which also coincides with the optical counterpart of Hulleman, van Kerkwijk, & Kulkarni (2000). We measure a pulse period consistent with the measurements of Gavriil & Kaspi (2001) and confirm limits to the amplitude of possible binary motion in a subset of period ranges previously investigated by (Wilson et al. 1999).

The superb *Chandra* spatial resolution allows us to determine that there is emission extending up to $100''$ from the pulsar, likely due to dust scattering. We are unable to

determine evidence for excess emission within a few arcseconds of the source (i.e., evidence for a plerion), due to contamination from the X-ray bright AXP and the associated dust scattering halo.

We thank H. Marshall for allowing us to compare our results with their observations prior to their publication, and for many insightful comments. This work was supported by grants MX-0101 and GO0-1018X (C.K.), NAG5-9350 (P.W.), GO0-1018X (S.P.).

REFERENCES

- Aldcroft, T. L., Karovska, M., Cresitello-Ditmar, M. L., Cameron, R. A., & Markevitch, M. L. 2000, *Proc. SPIE*, 4012, 650
- Anders, E. & Ebihara, M. 1982, *Geochim. Cosmochim. Acta*, 46, 2363
- Arnaud, K. 1996, in *ASP Conf. Ser. 101: Astronomical Data Analysis Software and Systems V*, G. H. Jacoby & J. Barnes (eds), 5, 17
- Bildsten, L. et al. 1997, *ApJS*, 113, 367
- Forman, W., Jones, C., Cominsky, L., Julien, P., Murray, S., Peters, G., Tananbaum, H., & Giacconi, R. 1978, *ApJS*, 38, 357
- Gaensler, B. M., Slane, P. O., Gotthelf, E. V., & Vasisht, G. 2001, *ApJ*, 559, 963
- Gavriil, F. P. & Kaspi, V. M. 2001, *ApJ* accepted
- Ghosh, P., Angelini, L., & White, N. E. 1997, *ApJ*, 478, 713
- Hulleman, F., van Kerkwijk, M. H., & Kulkarni, S. R. 2000, *Nature*, 408, 689
- Hulleman, F., Tennant, A. F., van Kerkwijk, M. H., Kulkarni, S. R., Kouveliotou, C., & Patel, S. K. 2001, *ApJ*, 563, L49
- Israel, G. L., Mereghetti, S., & Stella, L. 1994, *ApJ*, 433, L25
- Israel, G. L. et al. 1999, *A&A*, 346, 929
- Juett, A. M., Marshall, H. L., Chakrabarty, D., & Schulz, N. S. 2002, *ApJ*, 568, L31
- Kern, B. & Martin, C. 2001, *IAU Circular No. 7769*

- Markevitch, M. & Vikhlinin, A. 2001, in Submitted to ApJ,
astro-ph/010593
- Mereghetti, S. 1999, in *The NS-BH Connection*, astro-ph/9912207
- Mereghetti, S., Israel, G. L., & Stella, L. 1998, MNRAS, 296, 689
- Mereghetti, S. & Stella, L. 1995, ApJ, 442, L17
- Morrison, R. & McCammon, D. 1983, ApJ, 270, 119
- Paul, B., Kawasaki, M., Dotani, T., & Nagase, F. 2000, ApJ, 537, 319
- van Paradijs, J., Taam, R. E., & van den Heuvel, E. P. J. 1995, A&A, 299, L41
- White, N. E., Mason, K. O., Giommi, P., Angelini, L., Pooley, G., Branduardi-Raymont, G.,
Murdin, P. G., & Wall, J. V. 1987, MNRAS, 226, 645
- White, N. E., Angelini, L., Ebisawa, K., Tanaka, Y., & Ghosh, P. 1996, ApJ, 463, L83
- Wilson, C. A., Dieters, S., Finger, M. H., Scott, D. M., & van Paradijs, J. 1999, ApJ, 513,
464
- Wise, M. W., Huenemoerder, D. P., & Davis, J. E. 1997, in ASP Conf. Ser. 125: Astronomical
Data Analysis Software and Systems VI, Vol. 6, 477

Table 1. Phase Resolved Spectral Fits for 4U 0142+61

Model ID	Model Settings ^a		χ^2/ν	F -Test Probability ^b	
	$PL_{Norm} \propto BB_{Norm}$	kT_{BB} Linked			
1	Y	$0.458^{+0.003}_{-0.003}$	$3.35^{+0.02}_{-0.02}$	2009.428/1807	...
2	N	$0.465^{+0.003}_{-0.008}$	$3.39^{+0.01}_{-0.01}$	1993.472/1797	0.843
3	Y	N	$3.35^{+0.02}_{-0.02}$	1975.203/1798	0.9997
4	Y	$0.458^{+0.003}_{-0.003}$	N	1974.285/1798	0.9998
5	Y	N	N	1963.639/1789	0.9986 (0.624, 0.691) ^c

^aModel normalizations for each phase bin are free (unconstrained) to obtain its best fit value while N_H is linked (constrained to be identical at each phase) for all model variations. If the index or temperature are linked, then the best fit values are listed with 1σ uncertainties, else an “N” is listed indicating the parameters are not linked. The Temperature is listed in units of keV.

^bBased on the F -statistic, we claim that the given model is significantly better at the listed confidence levels. The probabilities are determined with respect to Model 1.

^cThe numbers in parentheses are the probabilities that Model 5 is significantly better than Models 3 and 4, respectively.

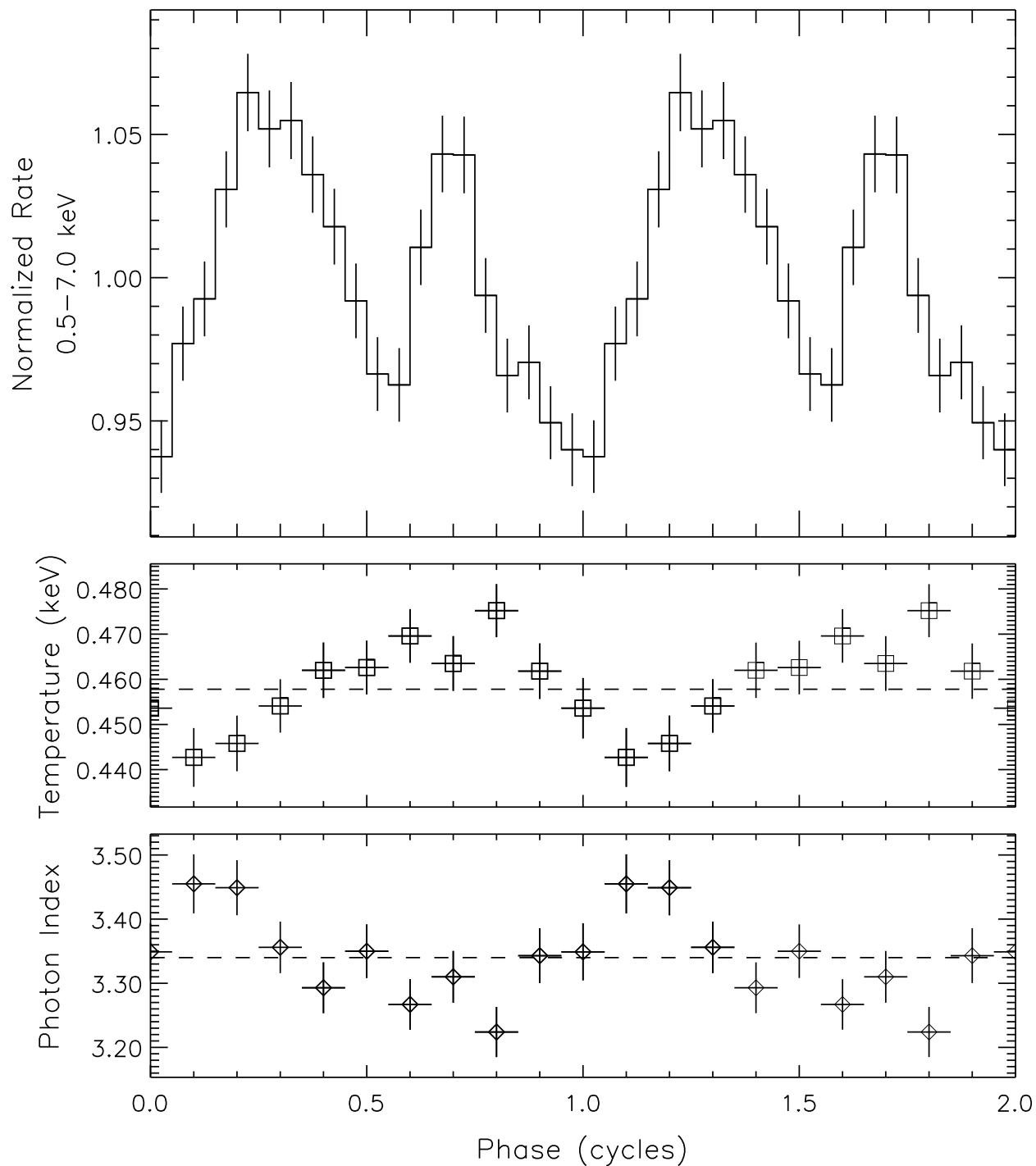


Fig. 1.— Top panel (a): The pulse profile of 4U 0142+61 (0.5 – 7.0 keV). Middle panel (b): Variation of the blackbody temperature from fitting each phase bin with a PL+BB model (Model 1). The phase averaged value is denoted by the dashed line (Model 5). Bottom panel(c) : Variation of the PL index (Model 1) and phase averaged value (Model 5: dashed line).

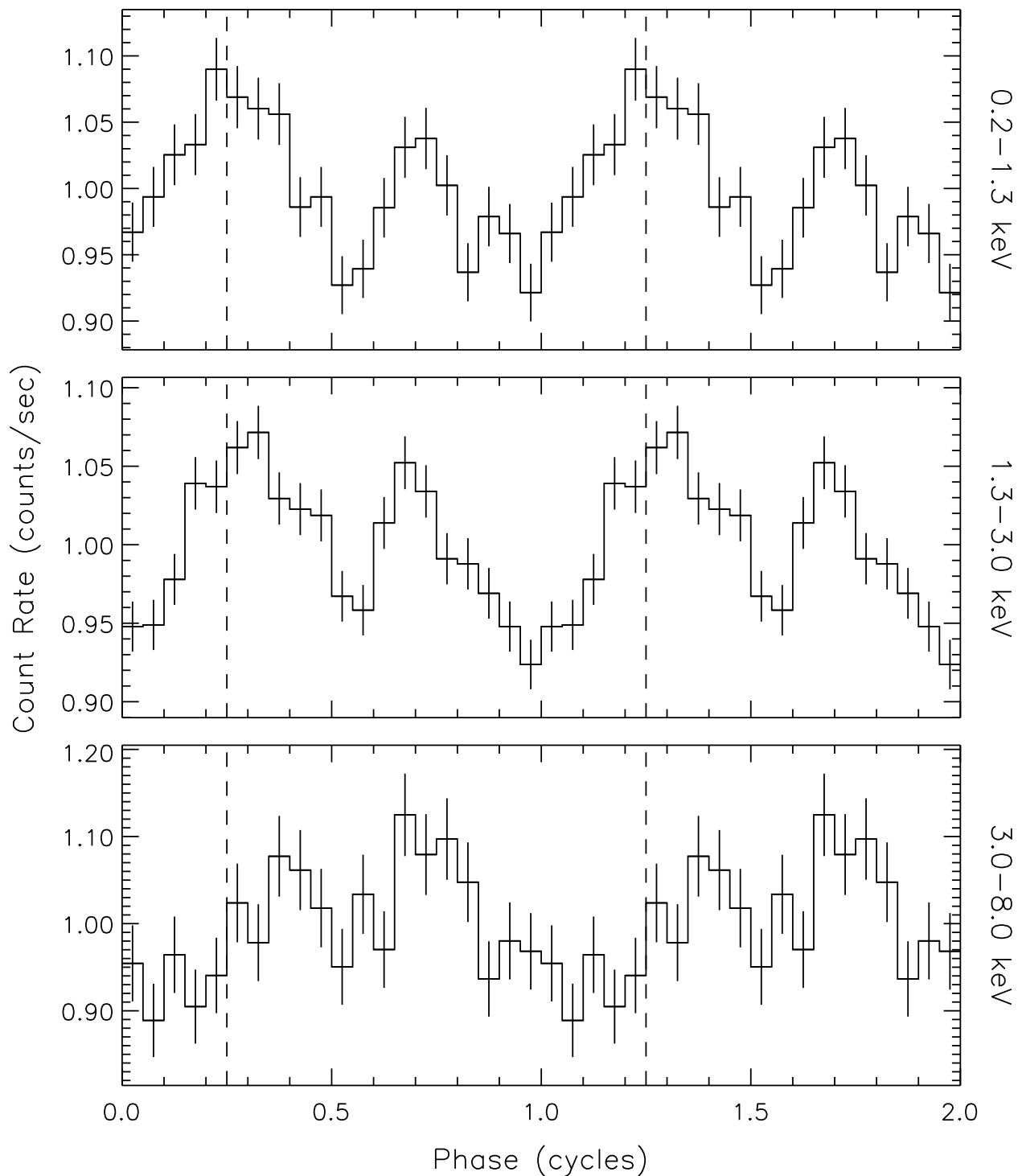


Fig. 2.— The pulse profile of 4U 0142+61 in three energy ranges. The RMS and peak to peak (PTP) values for each energy range are *Top*: 0.2 – 1.3 keV, $\text{RMS} = 4.6 \pm 0.5\%$, $\text{PTP} = 8.4 \pm 1.6\%$, *Middle*: 1.3 – 3.0 keV, $\text{RMS} = 4.1 \pm 0.4\%$, $\text{PTP} = 7.4 \pm 1.2\%$, and *Bottom*: 3.0 – 8.0 keV, $\text{RMS} = 5.6 \pm 1.0\%$, $\text{PTP} = 11.7 \pm 3.2\%$.

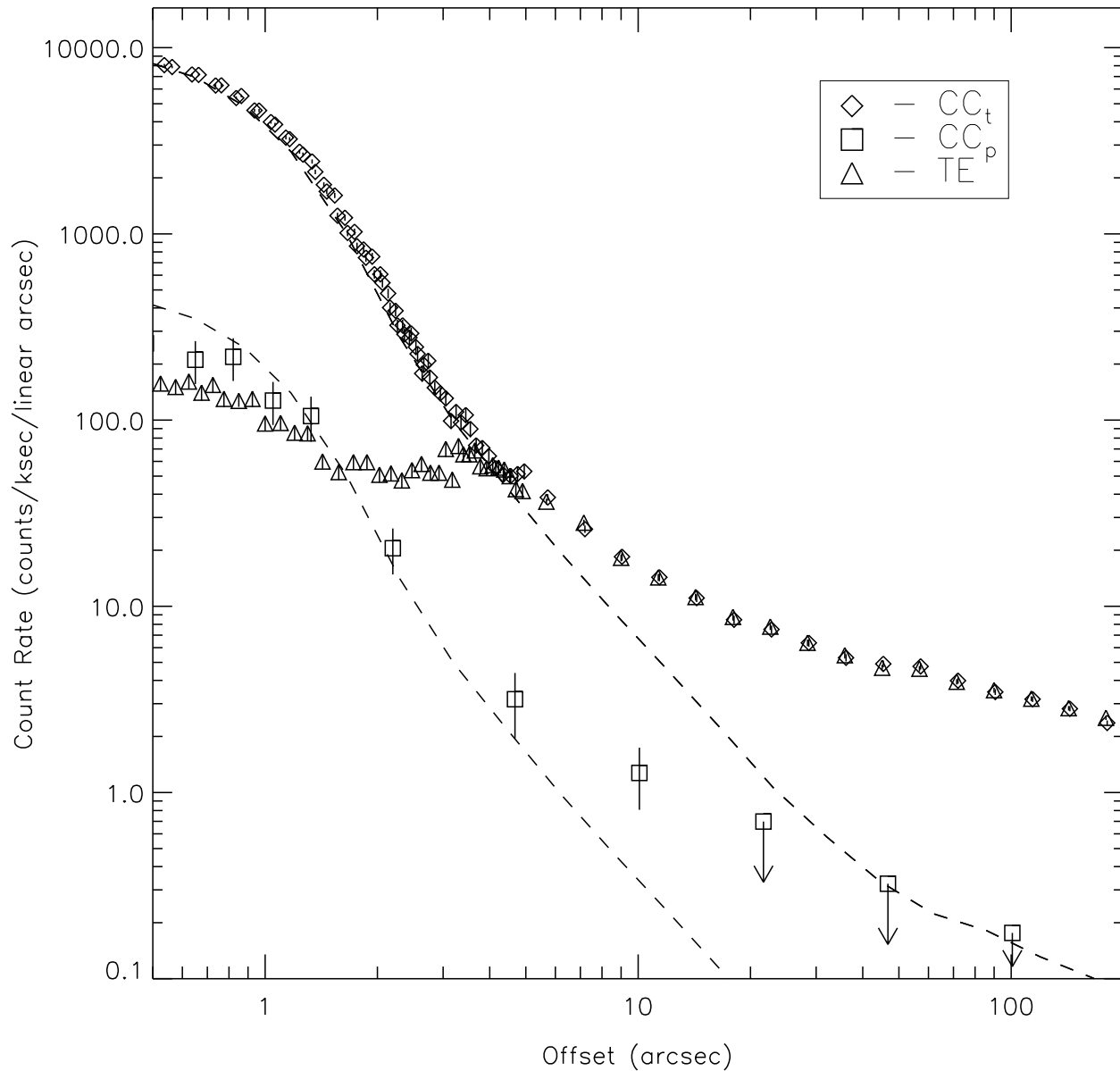


Fig. 3.— Radial surface brightness profiles of the total (CC_t) and pulsed (CC_p) emission (0.5–7.0 keV). The dashed lines are the simulated *Chandra* point spread function. Downward pointing arrows denote 2σ upper limits to the count rate. The triangles are TE mode data. Note the agreement between the total CC profile and the TE profile at radii $\gtrsim 4''$.

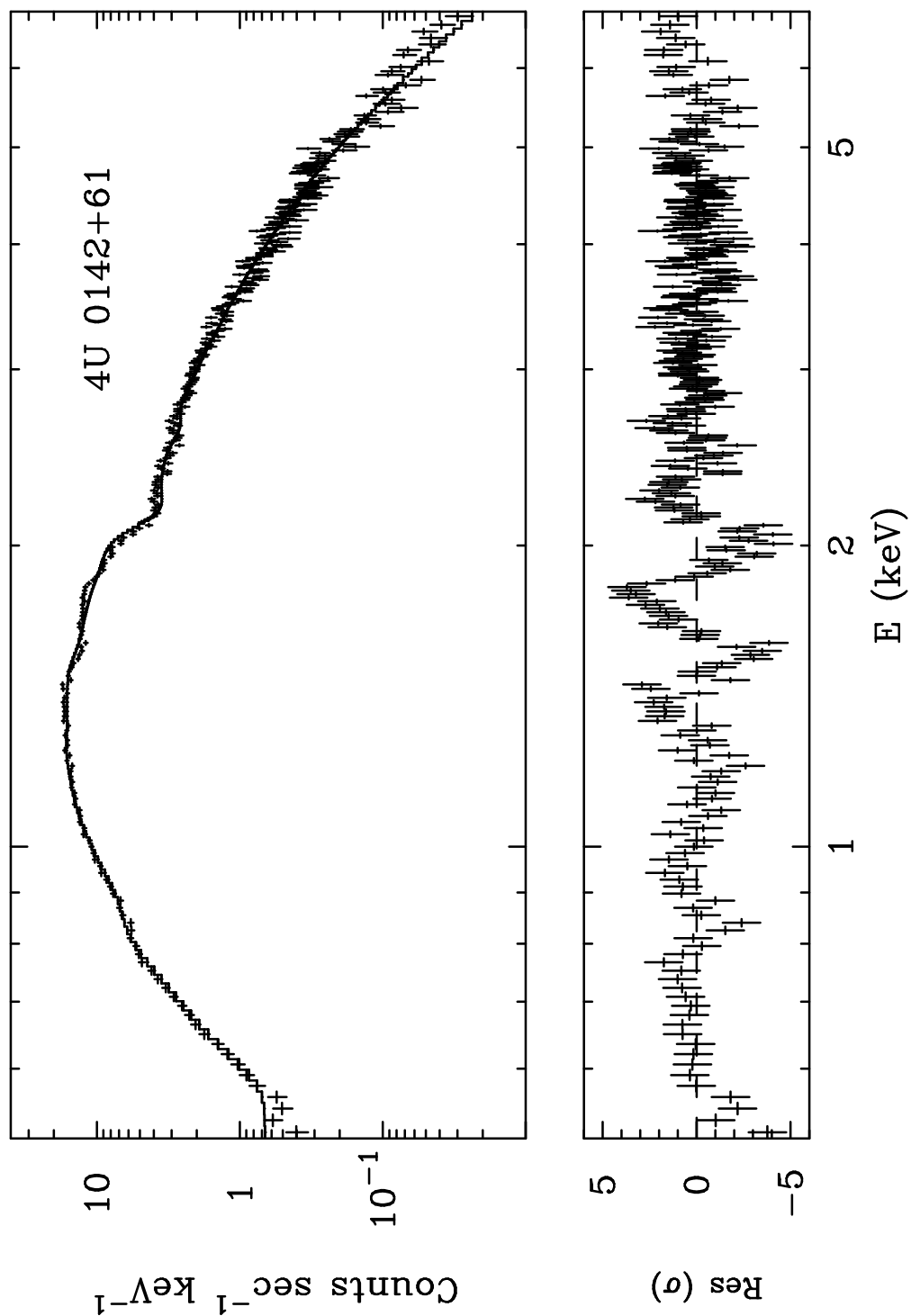


Fig. 4.— The best fit phase averaged spectrum of 4U 0142+61. The spectral data and model (PL+BB) are shown in the top panel and its residuals in units of σ are shown in the bottom panel. The feature at ~ 2.0 keV is due to a small shift of the location of the Ir absorption edge between the response and the data.